Structure of epitaxial (Fe,N) codoped rutile TiO2 thin films by x-ray absorption

T. C. Kaspar, A. Ney, A. N. Mangham, S. M. Heald, Yves Joly, V. Ney, Fabrice Wilhelm, Andrei Rogalev, F. Yakou, S. A. Chambers

Structure of epitaxial (Fe,N) codoped rutile TiO_2 thin films by x-ray absorption

T. C. Kaspar,[1,*] A. Ney,[2,†] A. N. Mangham,[1] S. M. Heald,[3] Y. Joly,[4] V. Ney,[2,†] F. Wilhelm,[5] A. Rogalev,[5] F. Yakou,[5] and S. A. Chambers[1]

[1]*Fundamental and Computational Sciences Directorate, Pacific Northwest National Laboratory, Richland, Washington 99354, USA*

[2]*Faculty of Physics and CeNIDE, University of Duisburg-Essen, 47057 Duisburg, Germany*

[3]*Advanced Photon Source, Argonne National Laboratory, Argonne, Illinois 60439, USA*

[4]*Institut Néel, CNRS et Université Joseph Fourier, BP 166, F-38042 Grenoble Cedex 9, France*

[5]*European Synchrotron Radiation Facility (ESRF), BP 220, 38043 Grenoble Cedex, France*

(Received 11 May 2012; revised manuscript received 2 July 2012; published 23 July 2012)

Homoepitaxial thin films of Fe:TiO_2 and (Fe,N):TiO_2 were deposited on rutile(110) by molecular beam epitaxy. X-ray absorption near edge spectroscopy (XANES) spectra were collected at the Ti L-edge, Fe L-edge, Ti K-edge, O K-edge, and N K-edge. No evidence of structural disorder associated with a high concentration of oxygen vacancies is observed. Substitution of Fe for Ti could be inferred, and secondary phases such as Fe_2O_3, Fe_3O_4, and $FeTiO_3$ can be ruled out. The similarity of the N K-edge spectra to O, and the presence of a strong x-ray linear dichroism signal for the N K-edge, indicates that N is substitutional for O in the rutile lattice and is not present as a secondary phase such as TiN. Simulations of the XANES spectra confirm substitution, although N appears to be present in more than one local environment. Neither Fe:TiO_2 nor (Fe,N):TiO_2 exhibit intrinsic room temperature ferromagnetism, despite the presence of mixed valent Fe(II)/Fe(III) in the reduced (Fe,N):TiO_2 film.

DOI: 10.1103/PhysRevB.86.035322 PACS number(s): 61.05.cj, 68.55.Ln, 75.50.Pp

I. INTRODUCTION

Efficient visible light photocatalysis could revolutionize hydrogen production, chemical synthesis, and pollution mitigation. Binary oxides such as TiO_2 have received much attention for these applications since they are stable under aqueous and oxidizing conditions and show promise as ultraviolet-light photocatalysts.[1,2] However, to operate in the visible portion of the solar spectrum, the wide bandgap of these oxides (3.0–3.2 eV for TiO_2) must be reduced. Anion doping of anatase TiO_2 by N shows promise as a means to reduce the bandgap into the visible region, resulting in visible-light photoactivity.[3] The photocatalytic activity of N-doped TiO_2, typically in the form of nanoparticles and powders, has subsequently been widely explored.[4–7] Recently, codoping schemes such as Fe cation doping along with N anion doping have been explored and in some cases have shown promise to increase photocatalytic activity.[8–11] Codoping is speculated to both promote visible light absorption and facilitate photogenerated charge separation and transfer.[8,11] However, in nanoparticles and fine powders, establishing the detailed mechanism of photocatalytic activity is significantly hindered by difficulties in determining the structural and electronic behavior of dopants.

Transition-metal-doped TiO_2 has also been extensively explored as a potential dilute magnetic semiconductor (DMS) for spintronics applications.[12] Recently, Fe-doped TiO_2 was shown to exhibit weak room-temperature ferromagnetism in films with reduced oxygen content.[13,14] The mechanism of ferromagnetic ordering was hypothesized to require the presence of Ti(III) defect states[14] or mixed-valent Fe(II)/Fe(III).[13] However, these studies did not characterize the spatial distribution or substitutional nature of the Fe dopant. Previous studies found that, with a relatively fast deposition rate, Fe dopants segregate to the film surface and form Fe_3O_4 clusters which provide a room temperature ferromagnetic signal.[15] To elucidate the mechanism of ferromagnetic ordering in these materials, careful and thorough materials characterization is necessary, particularly regarding the speciation and location of the transition metal dopants.

Recently, we showed[16] indirect evidence of N substitution in (Fe,N) codoped rutile TiO_2 homoepitaxial thin films deposited by plasma-assisted molecular beam epitaxy (PAMBE). A combination of characterization techniques indicated that N was present as N^{3-}, which appeared to be substitutional in the lattice. Codoping with N also increased the extent of Fe incorporation in the rutile lattice, reducing surface segregation of Fe dopants. Although optical absorption indicated a bandgap reduction to approximately 2.4 eV for N-doped TiO_2 and (Fe,N) codoped TiO_2, no significant visible light photocatalytic activity was observed for either film.

X-ray absorption (XAS) is a powerful technique to determine the charge state, structural environment, and electronic structure of materials in an atom-specific manner. Previous XAS studies of N-doped TiO_2 have focused on x-ray absorption near edge spectroscopy (XANES) of the O K-edge, Ti K-edge, Ti L-edge, and in some cases the N K-edge of N-doped anatase powders and nanoparticles. For example, Stewart *et al.*[17] found evidence of substantial O vacancy formation from both the O K-edge XANES and the pre-edge features of the Ti K-edge XANES. Changes to the electronic structure and atomic ordering were attributed to these vacancies and did not directly correlate with the small amount of N detected. Chen *et al.*[18] interpreted the N K-edge XANES of anatase reacted with NH_3 at various temperatures as substitutional N in a TiN-like environment, in addition to the presence of interstitial N. Reaction at higher temperatures produced a TiN secondary phase. Braun *et al.*[7] observed an additional feature in the pre-edge region of the O K-edge XANES, correlated with additional intensity in the Ti L-edge spectrum; with increasing N content, an increase in the relative amplitude of this feature and a decrease in visible light photoactivity were observed. Zhang *et al.*[6] utilized N and O K-edge XANES

and x-ray photoelectron spectroscopy (XPS), in addition to other techniques, to associate high visible light photoactivity with near-surface substitutional N species and neighboring O vacancies.

In this paper, we present XANES and x-ray linear dichroism (XLD) for the Ti K-edge, Ti L-edge, Fe L-edge, O K-edge, and N K-edge in the Fe-doped rutile TiO_2 (Fe:TiO_2) and (Fe,N) codoped rutile TiO_2 ((Fe,N):TiO_2) homoepitaxial thin films discussed in detail previously.[16] Analysis of epitaxial films provides substantial benefits compared to the study of nanoparticles to understand the fundamental role of dopants in a material, in particular due to the elimination of undercoordinated surface defects and surface-adsorbed species. The well-defined single crystal structure of epitaxial films also facilitates insightful XLD measurements, where the incident x-ray polarization is switched from parallel to perpendicular polarization relative to a given crystalline direction in the film; the difference in the XANES spectra arising from these signals is the XLD. X-ray linear dichroism is very sensitive to small changes in the fine structure of XANES, revealing subtle differences in local coordination and structure around the absorbing atom. In some cases, the XLD difference spectrum can be accurately modeled, allowing a quantitative measure of the number of dopants which are substitutional in the lattice.[19,20] By employing XLD difference spectra for O, N, and Ti in Fe:TiO_2 and (Fe,N):TiO_2, the structural and electronic role of N in rutile TiO_2 is elucidated. In addition, the dopant speciation and room temperature magnetic properties of Fe:TiO_2 and (Fe,N):TiO_2 are presented.

II. EXPERIMENTAL DETAILS

Fe-doped rutile TiO_2 and (Fe,N) codoped rutile TiO_2 homoepitaxial thin films were deposited on rutile(110) single crystals by PAMBE, as described previously.[16] Briefly, Fe and Ti were evaporated from effusion cells, and activated oxygen and nitrogen were supplied from the same electron cyclotron resonance microwave plasma source at an N_2:O_2 supply ratio of 3:1, maintaining a total chamber pressure of 2×10^{-5} Torr. Films were deposited at 550 °C to a thickness of approximately 500 Å. Two films are investigated in this study: $Fe_{0.02}Ti_{0.98}O_2$, which showed surface segregation of Fe by angle-resolved x-ray photoelectron spectroscopy (XPS), and $Fe_{0.02}Ti_{0.98}(O_{0.98}N_{0.02})_2$, which indicated no surface segregation of Fe.[16]

X-ray absorption spectra for the O K-edge, N K-edge, Ti L-edge, and Fe L-edge were collected on beamline ID08 of the European Synchrotron Radiation Facility (ESRF); spectra were collected in total electron yield (TEY) mode to minimize signal from the underlying rutile substrate. The Ti K-edge spectra were collected on beamline ID12 in fluorescence yield (FY) mode. Due to interference with the Ti K-edge, the weak Fe K-edge signal could not be measured. The incident x-rays were perpendicular to the sample surface, and the electric field vector (**E**) was aligned either parallel or perpendicular to the *c* axis of the film by flipping the linear polarization of the synchrotron light from vertical to horizontal using either a quarter wave plate (ID12) or the undulator (ID08). For rutile TiO_2(110) films, the *c* direction ([001]) lies in the plane of the film, and the in-plane direction perpendicular to the *c* direction is the [1$\bar{1}$0] direction [see inset to Fig. 1(a)]. Unless noted otherwise, spectra were normalized with respect to the edge jump. The powder-averaged XAS spectra were calculated as

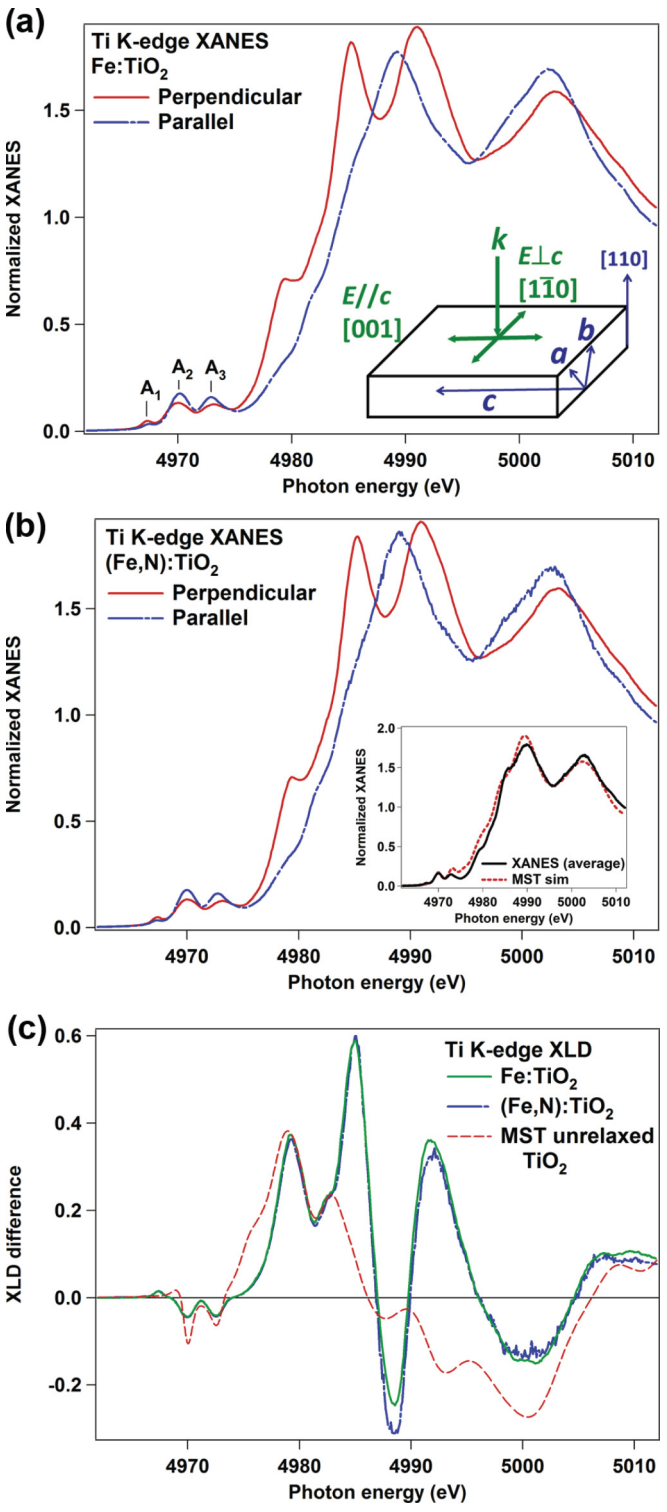

FIG. 1. (Color online) Self-absorption-corrected Ti K-edge XANES spectra for (a) Fe:TiO_2 and (b) (Fe,N):TiO_2. Inset in (a) sketches parallel and perpendicular polarizations. Inset in (b) compares averaged XANES spectrum with multiple-scattering simulation of unrelaxed TiO_2. (c) XLD difference spectra, along with multiple scattering simulation of unrelaxed TiO_2.

([001] + 2*[1$\bar{1}$0])/3.[21] The Ti K-edge spectra collected in FY were corrected for self-absorption effects by taking into account the chemical composition and density, the essentially infinite thickness of the bulk sample, the various background contributions (fluorescence of subshells and matrix as well as coherent and incoherent scattering), the angle of incidence of the x-ray beam, and the solid angle of the detectors.[22] The XLD spectra were calculated as [1$\bar{1}$0]–[001].

The XANES spectra and XLD difference spectra were simulated using the FDMNES code.[23] FDMNES can utilize two different density functional theory (DFT) techniques to calculate the x-ray absorption final states: multiple scattering theory (MST) with approximate potentials or the more precise finite difference method (FDM) with full potentials. The Ti and Fe L edges are qualitatively simulated utilizing MST with muffin tin (MT) potentials. Simulation of the O and N K edges are the primary focus of the current study and are calculated using FDM with a self-consistent evaluation of the electronic structure. We have confirmed that this is required in order to obtain good agreement with experiment.

For the simulations, a 2 × 2 × 3 supercell (24 Ti, 48 O) of rutile was utilized; one cation in the center was replaced with Fe (except when simulating N:TiO_2), and an adjacent anion was replaced with N. This rigid structure is referred to below as "unrelaxed". For the "relaxed" structure, the supercell was allowed to relax in three dimensions, as described previously.[16] However, upon relaxation the fourfold axis relaying the chains of octahedra in rutile[24] is lost, and the [110] and [1$\bar{1}$0] directions are no longer equivalent. This is artificial because, at these low doping levels, long-range ordering of the dopants is not expected, and thus the dopants substitute with equal probability in Jahn–Teller distorted oxygen octahedra whose distortions lie along either [110] or [1$\bar{1}$0]. To recover the fourfold experimental axis, which exhibits an isotropic dependence on polarization in the *ab* plane, the simulated spectra for polarization along [110] and [1$\bar{1}$0] must be averaged. Therefore, the powder-averaged simulated XAS spectra were calculated as ([001] + [1$\bar{1}$0] + [110])/3, and the simulated XLD spectra were calculated as ([110] + [1$\bar{1}$0])/2 − [001].

To increase the signal for room-temperature magnetic measurements, thicker films of Fe:TiO_2 and (Fe,N):TiO_2 (2000 Å) were deposited under the same conditions as above. To reduce external sources of magnetic contamination, the rutile(110) substrates were etched in concentrated HNO_3 (back and sides only) before deposition; residual ferromagnetic signals were $<5 \times 10^{-6}$ emu. X-ray photoelectron spectra were collected with a GammaData/Scienta SES 200 analyzer and a monochromatic Al Kα X-ray source. A low-energy electron flood gun was utilized for compensation of sample charging. The Fe K-edge XANES was measured for the thick (Fe,N):TiO_2 film at PNC-CAT beamline 20-BM at the Advanced Photon Source (APS); perpendicularly polarized x-rays were incident on the sample at a grazing angle, and sample spinning was employed to reduce Bragg diffraction effects. With this measurement geometry, sufficient Fe K-edge signal could be collected on the thick doped films. Magnetic properties were measured at room temperature by vibrating sample magnetometry (VSM) with the magnetic field applied in the plane of the film.

III. RESULTS AND DISCUSSION

A. X-ray linear dichroism of Ti and Fe

The Ti K-edge XANES spectra in both vertical and horizontal polarizations are shown in Fig. 1(a) for Fe:TiO_2 and Fig. 1(b) for (Fe,N):TiO_2; all spectra have been corrected for self-absorption. As expected for single-crystal films, the XANES fine structure depends on the polarization of the incident x-rays when aligned either parallel or perpendicular to the *c* direction. The inequivalent bonding environments sensed in these two orientations give rise to differences in XANES fine structure, as observed previously for rutile(110).[25] The position of the absorption edge inflection point at ~4981 eV indicates Ti is present as Ti(IV)[26] with no evidence of reduced Ti(III). The relative intensities of the three pre-edge peaks, labeled A_1, A_2, and A_3 in Fig. 1, are consistent with the rutile crystal structure.[26] The nature of the transitions (dipole or quadrupole) giving rise to these pre-edge peaks has been controversial.[26,27] However, recent density functional theory (DFT) calculations[28] have strongly supported the interpretation[25,27] that peak A_1 is due to a quadrupole transition from 1*s* to 3*d* (t_{2g}) in the Ti absorber, peak A_2 arises from a dipole transition from 1*s* to hybridized *p*-*d* (t_{2g}) on the neighboring Ti [for **E** parallel to *c*, there is also a small contribution from the quadrupole 1*s* to 3*d* (e_g) transition of the Ti absorber], and peak A_3 is a dipole transition from 1*s* to hybridized *p*-*d* (e_g) on the neighboring Ti. The small additional quadrupole contribution to A_2 in the parallel polarization can be seen as a relative increase in the intensity of A_2 compared to A_1 and A_3 in this polarization in Figs. 1(a) and 1(b).

The XLD is calculated as the direct difference between the XANES spectra at the two polarizations and is shown in Fig. 1(c) for both Fe:TiO_2 and (Fe,N):TiO_2. The strong similarity in the XLD signals for Fe:TiO_2 films with and without N codoping indicates that adding a small fraction of N does not substantially disrupt the rutile lattice. In addition, because of the bulk sensitivity of FY in the hard x-ray regime, the XANES and XLD spectra also contain a considerable fraction of signal stemming from the underlying rutile substrate. Figure 1(c) shows an FDMNES multiple scattering simulation within the muffin-tin approximation utilizing self-consistent potentials of the XLD signal from unrelaxed, undoped TiO_2. Comparison of the powder-averaged XANES spectrum with the simulation is given in the inset to Fig. 1(b). The MST simulation reproduces the experimental XANES spectrum fairly well, although the agreement in the pre-edge region and along the leading edge is not as good as previous simulations with the FDMNES code using the finite difference method (FDM).[25] The poor agreement leads to a clear discrepancy between experiment and simulation for the XLD spectrum in the range of 4980 to 5000 eV. This is in contrast to wurtzite GaN or ZnO, where the muffin-tin approximation works rather well to simulate the XLD spectrum.[19,20]

The Ti L-edge absorption spectrum, collected in TEY mode, is plotted in Fig. 2(a) for (Fe,N):TiO_2. The L-edge spectra of 3*d* metals such as Ti are dominated by the dipole 2*p*-3*d* transition. Spin-orbit splitting of the 2*p* orbitals into $2p_{3/2}$ (L_3) and $2p_{1/2}$ (L_2), and crystal field splitting of the 3*d* orbitals into e_g and t_{2g}, results in a manifold of four absorption peaks for

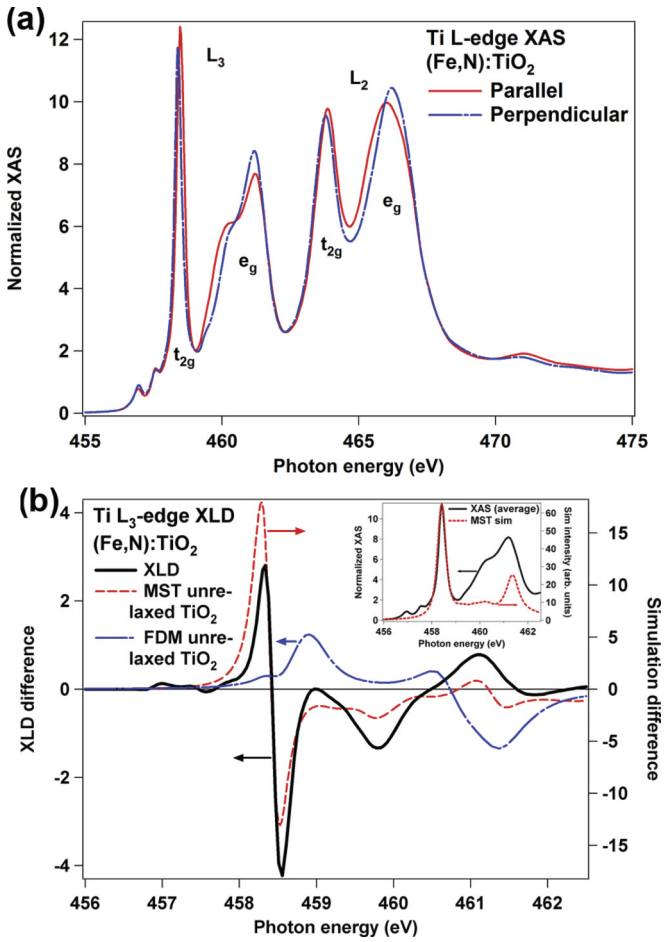

FIG. 2. (Color online) (Fe,N):TiO_2 Ti L-edge (a) XAS and (b) XLD. Multiple-scattering simulation of unrelaxed TiO_2 is given for XLD in (b) and powder-averaged XAS in the inset. FDM simulation of XLD is shown for comparison in (b).

the Ti L-edge of TiO_2. The e_g states are further split due to the tetragonal distortion from perfect octahedral symmetry, which occurs for both anatase and rutile. However, the intensity ratio of the split peaks is opposite for the two crystal structures; the TiO_2 L_3 spectrum presented in Fig. 2(a) indicates the higher-energy e_g peak is more intense than the lower-energy peak, consistent with previous reports of rutile L-edge spectra.[29]

Braun *et al.*[7] observed an additional feature in the Ti L-edge spectra which increased with increasing N content in N-doped anatase nanopowders. This new feature, located between the t_{2g} and e_g peaks, was tentatively assigned as the contribution from the $2p$-$3d$ (e_g $d_z{}^2$) transition, arising from the substantial quantity of oxygen vacancies introduced with N doping during nanoparticle synthesis. In the present work, the lack of Ti^{3+} observed by XPS, as well as the transparency of the films, indicates that a comparable quantity of oxygen vacancies are not present despite the relatively high N concentration (2.8 anion% or 1.9 at%). Likewise, the e_g $d_z{}^2$ feature observed by Braun *et al.* is not present in the Ti L-edge spectrum in Fig. 2(a).

The XLD difference for the Ti L_3 edge is plotted in Fig. 2(b). The FDMNES MST simulation within the muffin-tin approximation of the XLD signal for unrelaxed, undoped TiO_2 results in qualitative agreement with the experimental data. The main features of the XLD are reproduced, although the predicted intensity is approximately six times higher than the experimental value. The inset shows the powder-averaged XAS spectrum and the MST simulation of the XAS; the t_{2g} region is well reproduced (except for the mismatched intensity), but the first peak in the e_g region is underestimated by the simulation. The theoretical framework necessary to simulate the $L_{2,3}$ edges of transition metals such as Ti and Fe is in principle more complex than that required to describe the K edges, since for the $L_{2,3}$ edges, the photoelectron probes localized orbitals, and multielectronic phenomena can dramatically influence the spectra. Even for Ti(IV), which is $3d^0$ and thus not expected to present "multiplet" features, the experimental branching ratio between L_3 and L_2 is far from the expected value of 2:1 [see Fig. 2(a)], indicating multiplet effects are occurring. For these reasons, it might be expected that a full FDM simulation would be necessary to accurately reproduce the Ti L-edge features. Unexpectedly, however, the full FDM simulation (without self-consistent potentials) shown in Fig. 2(b) reproduces the experimental Ti L-edge much more poorly than the MST simulation. Including self-consistent potentials decreases the quality of the fit even further (not shown). It is unclear why the FDM simulation fails to reproduces the Ti L-edge satisfactorily. A time-dependent DFT (TD-DFT) approach utilizing a Hubbard correction may be useful to accurately reproduce the experimental L edges; however, this is beyond the scope of the present work.

The Fe L-edge absorption spectrum for (Fe,N):TiO_2 is shown in Fig. 3(a). These spectra do not closely match the Ti L-edge spectra shown in Fig. 2(a), which is to be expected considering the different electron configuration of Fe(III) ($3d^5$) compared to Ti(IV) ($3d^0$). Thus, a simple line shape comparison with the Ti spectra cannot determine whether the Fe dopants are substitutional in the rutile lattice. Notably, however, the Fe L-edge spectra in Fig. 3(b) exhibit fine structure at both the L_3 and L_2 edges, in contrast to the L-edge spectra for metallic Fe, where any fine structure at the L_3 and L_2 edges is absent. While the L_3 and L_2 peak positions do not differ significantly for Fe(II) and Fe(III), the fine structure is sensitive to the local environment of the absorber. The fine structure of the Fe L-edge spectra in Fig. 2(a) are not similar to reference spectra of α-Fe_2O_3 (hematite),[30] Fe_3O_4 (magnetite),[31] or $FeTiO_3$ (ilmenite),[31,32] indicating that the majority of Fe is not present as a secondary phase of Fe_2O_3, Fe_3O_4, or $FeTiO_3$ in (Fe,N):TiO_2. In addition, the Fe L-edge signal is rather weak despite the use of the surface-sensitive TEY mode to collect the spectra; this excludes a significant Fe-enrichment at the surface, which would lead to a much more pronounced Fe signal. These results are consistent with previous XPS spectra for these samples,[16] which indicated that Fe occurs exclusively as Fe(III) with little surface segregation. Combining the XPS and L-edge XAS data, Fe substitution for Ti in the rutile lattice can be inferred.

Small differences are observed in the Fe L-edge spectra at the two x-ray polarizations, leading to a weak XLD signal, which is plotted in Fig. 3(b). The presence of an XLD signal implies that at least a portion of the Fe dopants are

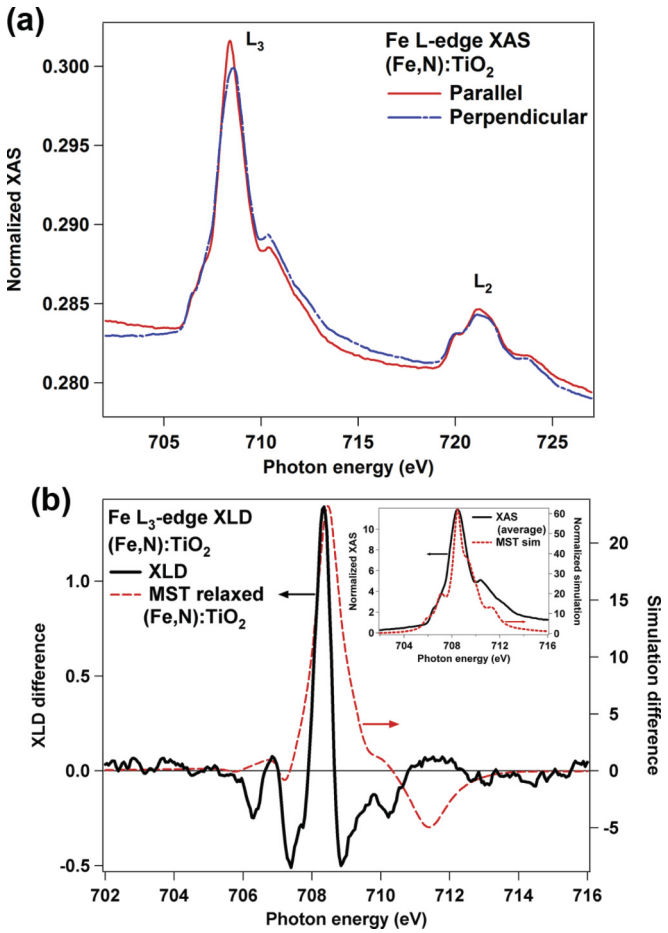

FIG. 3. (Color online) Fe L-edge (a) XAS and (b) XLD. Multiple-scattering simulation of relaxed (Fe,N):TiO_2 is given for XLD in (b) and powder-averaged XAS in the inset.

preferentially oriented in the film and not in the metallic form, consistent with the visible fine structure in the XAS. However, the strong and inhomogeneous background in the weak XAS spectra at the two polarizations is difficult to remove completely and thus may influence the XLD difference spectrum. A multiple scattering simulation of the XLD of (Fe,N):TiO_2 is also shown in Fig. 3(b); the powder-averaged XAS spectrum is compared to experiment in the inset of Fig. 3(b). Similar to the Ti L-edge, the simulated XAS spectrum matches the experimental line shape reasonably well for the main L_3 peak (except for an overestimation of the intensity), but not the fine structure above 710 eV. In contrast to the simulation of the Ti L-edge, the agreement between simulation and experiment for the Fe L-edge XLD is poor, with only the main peak reproduced, although with a much higher intensity. Again, this is likely due to the multielectronic phenomena mentioned above. It may also arise in part from structural disorder in the Fe cations; previous characterization of Fe in the (Fe,N):TiO_2 film found evidence of Fe substitution, but significant disorder in the film when investigating both Fe and Ti with Rutherford backscattering spectrometry rocking curves.[16] Nonetheless, the qualitative reproduction of the main XLD peak supports the assignment that Fe is predominantly substitutional for Ti and not present as secondary phases, interstitials, or on antisite locations.

B. X-ray linear dichroism of O and N

Figure 4(a) shows the O K-edge XANES spectra for (Fe,N):TiO_2 in both parallel and perpendicular polarizations. Again, strong anisotropy is observed, indicative of

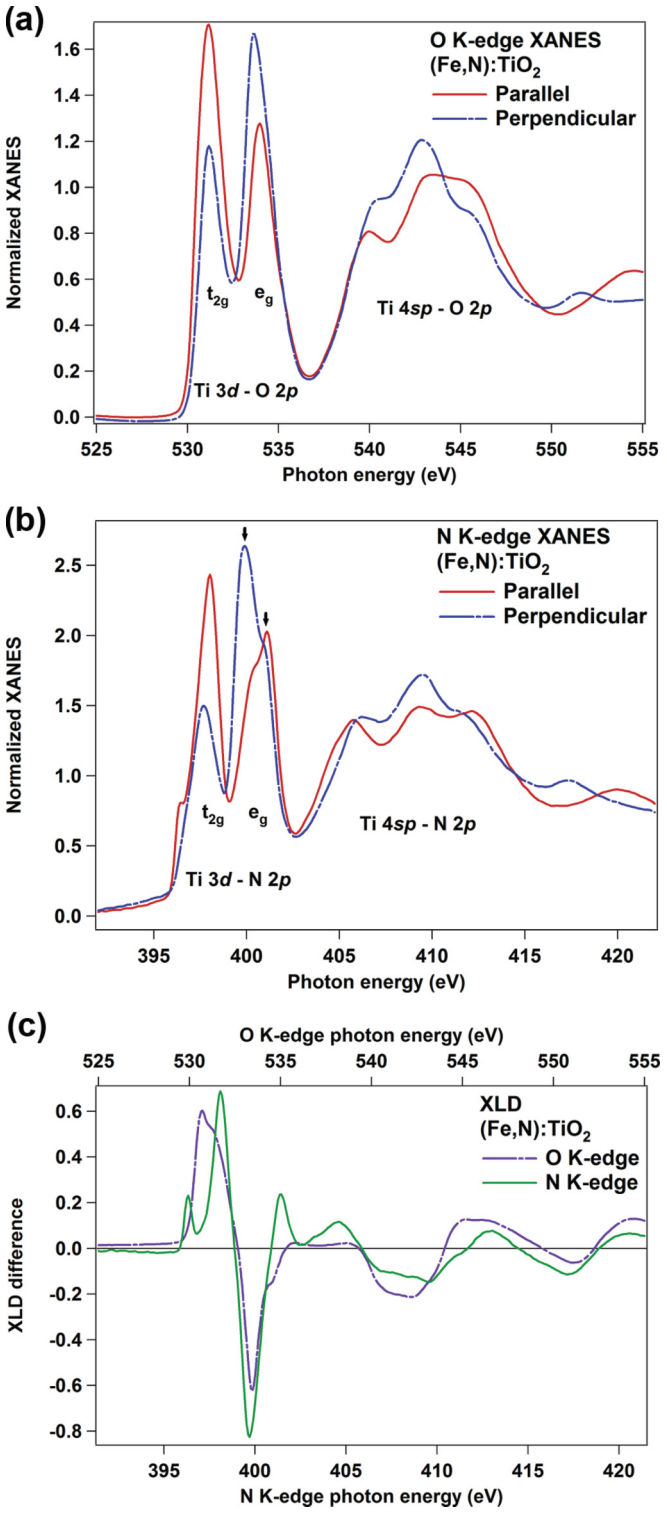

FIG. 4. (Color online) K-edge XANES of (Fe,N):TiO_2 for (a) O and (b) N. Arrows indicate double-peak structure of second pre-edge peak. (c) Experimental XLD difference spectra for the O and N K-edges.

well-ordered oxygen anions in the single-crystal lattice. Previous studies on N:TiO_2 nanoparticles found a loss of fine structure in the O K-edge, which was attributed to the presence of a substantial fraction of oxygen vacancies.[17] The prominent fine structure in Fig. 4(a) implies that the concentration of oxygen vacancies formed during film synthesis is much less than in previous nanoparticle work[17] and is below the detection limit of O K-edge XANES. The O K-edge of TiO_2 is understood to consist of two strong pre-edge peaks arising from transitions from O 1*s* to hybridized Ti 3*d*-O 2*p* orbitals; the Ti 3*d* orbitals are further split into t_{2g} and e_g components. The main absorption edge arises from O 1*s* to hybridized Ti 4*sp*-O 2*p* transitions.[33] As with the Ti absorption edges, differences in the distortion from octahedral symmetry for the anatase and rutile crystal structures leads to slight changes in the O K-edge line shape, particularly past the main absorption edge.[34] As expected, the measured O K-edge XANES line shape for (Fe,N): TiO_2 is consistent with that reported for rutile[34,35] [see also the inset to Fig. 5(a) below].

Correlated with the additional feature observed in the Ti L-edge spectra, Braun *et al.*[7] observed an additional feature between the t_{2g} and e_g peaks of the O K-edge spectra of N:TiO_2 anatase nanopowders, assigned as a transition to the e_g d_z^2 orbital. The lack of such a feature in Fig. 4(a) confirms the lack of oxygen vacancies present in the (Fe,N):TiO_2 films. It should be noted, however, that the increase of the additional feature was found to correlate with reduced photocatalytic activity; the highest activity was found for the nanopowders with the lowest N content and smallest e_g d_z^2 feature.[7] In contrast, the (Fe,N):TiO_2 films contain a relatively high concentration of N without producing the e_g d_z^2 feature, but no visible light photoactivity was detected.[16]

The N K-edge XANES spectra for (Fe,N):TiO_2 are shown in Fig. 4(b). The line shape of the N K-edge spectra are qualitatively similar to previous results for N in anatase TiO_2[18] and in TiN.[36] The spectra exhibit similar fine structure to the O K-edge XANES spectra in Fig. 4(a), particularly past the main absorption edge, providing evidence that N occupies a similar crystalline environment as O in the rutile lattice. No evidence of interstital N_2, with a sharp peak at 401.4 eV,[36] is seen. Likewise, XANES spectra collected in fluorescence yield (not shown), which is bulk sensitive, did not reveal the signature of interstitial N_2 in the bulk of the film. By analogy to the O K-edge, the pre-edge peaks can be assigned as transitions from N 1*s* to hybridized Ti 3*d*-N2*p* orbitals; again, the Ti 3*d* orbitals are split into t_{2g} and e_g components. The main absorption edge is assigned as transitions from N 1*s* to hybridized Ti 4*sp*-N 2*p* orbitals. In contrast to the O K-edge spectra, the e_g pre-edge peak for the N K-edge appears to have a double-peak structure, as illustrated by arrows in Fig. 4(b).

The N K-edge spectra presented in Fig. 4(b) vary markedly from the XANES spectra presented by Zhang *et al.* for samples processed at $\leqslant 500\,^{\circ}$C, which were assigned to substitutional near-surface N in TiO_2. However, the N 1*s* binding energy observed by XPS for substitutional N in (Fe,N):TiO_2, 396.0 eV,[16] matches the binding energy observed by Zhang *et al.*, 395.7 eV, reasonably well. The N 1*s* binding energy in TiN is reported to be 397.0–397.4 eV,[37,38] which shifts to lower binding energy (∼396 eV) as the TiN film is oxidized and presumably forms an oxynitride.[37] In polycrystalline samples such as the nanoparticle powders studied previously,[6,18] it can be difficult to distinguish from the N K-edge XANES spectrum whether N is substitutional in TiO_2 or forms a secondary phase of TiN. The advantage of single-crystal epitaxial films is the ability to probe the crystalline anisotropy through the incident x-ray polarization. If an N-containing secondary phase of any type exists in the lattice as randomly oriented crystalline grains, it will not exhibit crystalline anisotropy when the x-ray polarization is changed. Even if TiN, which is the most likely secondary phase in N:TiO_2, were present with a single, epitaxial orientation, its cubic crystal structure would not exhibit crystalline anisotropy when the incident x-ray polarization is switched to an orthogonal direction. However, the N K-edge XANES data in Fig. 4(b) clearly exhibits anisotropy. This is seen quantitatively by plotting the XLD signal as in Fig. 4(c). The presence of a clear XLD signal itself provides strong evidence that the majority of N is substitutional in the rutile lattice; any secondary phases are negligibly small. The experimental N XLD data matches well with the O XLD in Fig. 4(c), implying that N is substitutional for O in (Fe,N):TiO_2.

Further corroboration that N substitutes for O in the (Fe,N):TiO_2 film is provided by FDM simulations of both the O and N K-edge XANES and XLD. For ease of comparison, both the O and N K-edge experimental and simulated spectra have been normalized to the tallest peak in the main absorption region for the perpendicular polarization. These simulations are shown in Fig. 5. The simulations of unrelaxed (Fe,N):TiO_2 predict XANES and XLD signals for the O K-edge, which are quantitatively similar to those observed experimentally [Fig. 5(a)]. For the N K-edge, the agreement between experiment and simulation reveals subtleties in the local environment around N. Figure 5(b) plots the powder-averaged experimental N K-edge spectra, as well as FDM simulations using both relaxed and unrelaxed TiO_2 structures, with and without the presence of Fe in addition to N. In all cases, the simulations semiquantitatively reproduce the primary features of the experimental spectra, including the t_{2g} and e_g pre-edge peaks and the structure of the main absorption edge. As shown above in Fig. 4(b), the experimental N K-edge XANES spectra in both polarizations show a double-peak structure in the e_g pre-edge peak, which is retained in the averaged data. Finite difference method simulations of the N K-edge do not reproduce this double-peak structure. However, the simulations show relative energy shifts of the single e_g peak depending on the details of the simulation, indicating that the experimental spectrum likely arises from a convolution of various local environments around the N absorber. The position of the e_g pre-edge peak appears to correlate with whether the structure is relaxed or not, regardless of the presence of neighboring Fe. It should be noted that the (Fe,N):TiO_2 structure was allowed to relax in three dimensions, without consideration of the epitaxial constraint of the substrate, and only one Fe-N dopant configuration was considered. Thus, the relaxed structure determined by DFT total-energy calculations may not precisely reflect the relaxed (Fe,N):TiO_2 film structure.

Discrepancies between the experimental and simulated N K-edge XANES can be more clearly seen when comparing the experimental and simulated XLD difference spectra, as shown in Fig. 5(c). The FDM simulations of unrelaxed (Fe,N):TiO_2

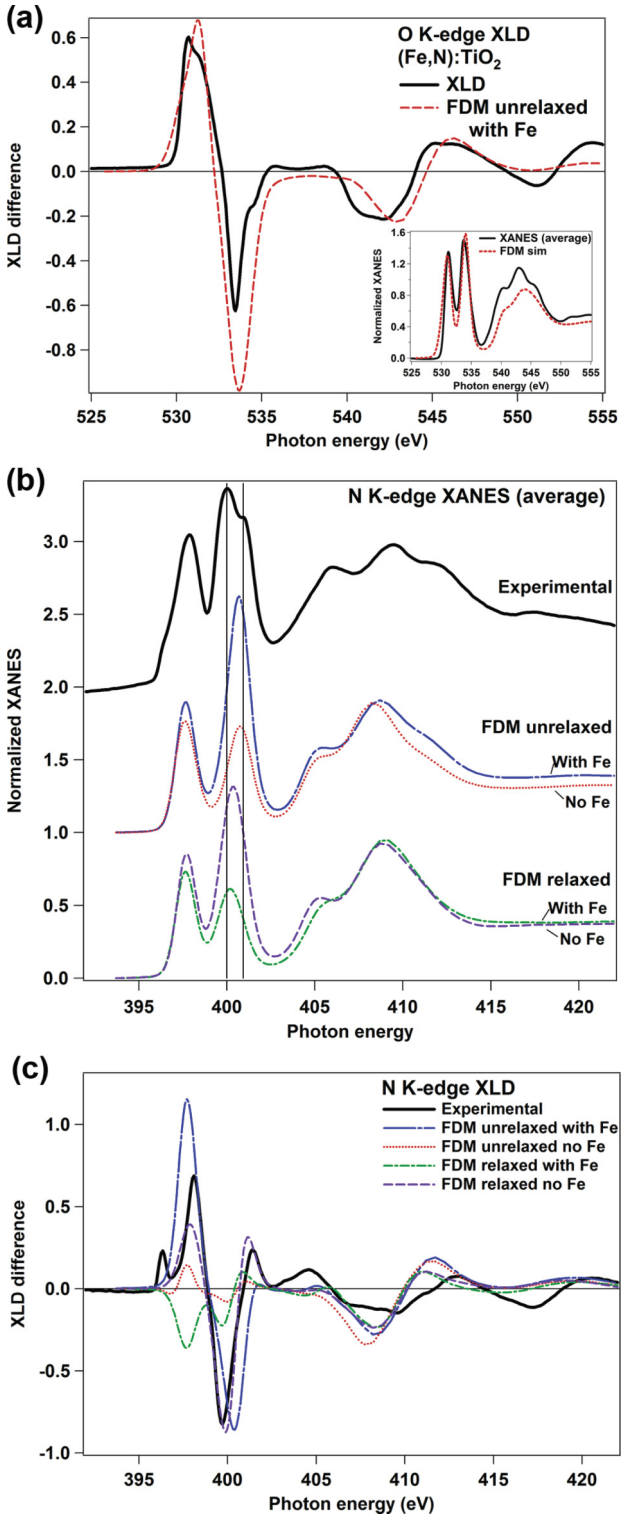

FIG. 5. (Color online) (a) O K-edge XLD of (Fe,N)TiO_2 and FDM simulation of unrelaxed (Fe,N):TiO_2. Inset: Averaged O K-edge XANES comparison. (b) Comparison of N K-edge XANES of (Fe,N):TiO_2 with FDM simulations. (c) N K-edge XLD of (Fe,N):TiO_2 with FDM simulations.

and relaxed N:TiO_2 appear to match the experimental XLD signal fairly well, while relaxed (Fe,N):TiO_2 and unrelaxed N:TiO_2 do not reproduce the pre-edge region. For all models, the main absorption region above ~405 eV agrees well with the experimental XLD. The success of these models to reproduce the main features of the N K-edge clearly indicates that the majority of N is substitutional in the rutile lattice, although more advanced modeling would be required to quantify the fraction of substitutional N and the precise local environment.

The presence of strong XLD at the N K-edge, providing direct evidence of N substitution for O in the rutile lattice, is consistent with previous nuclear reaction analysis (NRA) measurements in the channeling geometry for both N:TiO_2 (Ref. 39) and (Fe,N):TiO_2.[16] The substitution of N for O in the lattice implies that N participates in the electronic structure of Fe:TiO_2, at least locally. Despite this, however, no ultraviolet (UV) or visible light photoactivity was observed for (Fe,N):TiO_2 homoepitaxial thin films. This inactivity has been attributed to hole-trapping at N sites, and carrier recombination at defects may also play a detrimental role.[16]

C. Magnetic properties of thick Fe:TiO_2 and (Fe,N):TiO_2

To elucidate whether a uniform depth distribution of Fe dopants in TiO_2, achieved by codoping with N, will induce intrinsic room temperature ferromagnetism attributable to substitutional Fe(II) and/or Fe(III), thick films of Fe:TiO_2 and (Fe,N):TiO_2 were deposited on magnetically clean substrates and measured by VSM. As expected from analysis of the thin films discussed above,[16] the Fe:TiO_2 film showed extensive surface segregation of Fe; by *in situ* XPS, the cation fraction [Fe/(Fe + Ti), corrected for photoemission cross section[40]] increased from 0.04 to 0.19 when the photoelectron takeoff angle was changed from the sample normal to low-angle emission (12° off the surface plane). In contrast, the (Fe,N):TiO_2 film showed less surface segregation, with an increase in Fe cation fraction from 0.02 (normal) to 0.06 (12°). The corrected[40] anion fraction N/(N + O) was 0.028 at both normal and 12° takeoff angles. The thick Fe:TiO_2 sample was transparent, as were the thinner samples discussed above. However, the thick (Fe,N):TiO_2 film was dark blue, indicating reduction of the oxide. Comparison of the Ti 2*p* core level XPS spectra in Fig. 6(a) for (Fe,N):TiO_2 and Fe:TiO_2 reveals spectral intensity at lower binding energy for (Fe,N):TiO_2, which is not present for Fe:TiO_2. This intensity can be fit with a Voigt peak placed ~0.9 eV below the main peak, indicating it is due to $TiO_{5-\delta}N_{1+\delta}$ bonding, not the presence of Ti(III).[16,39] The N 1*s* spectra shown in the inset to Fig. 6(a) indicate that N is present primarily as substitutional N_O with a binding energy of ~396 eV.[16]

In contrast to the thick Fe:TiO_2 film and the thin (Fe,N):TiO_2 films discussed above, the Fe 2*p* core level spectra for the thick (Fe,N):TiO_2 film indicates substantial reduction of the Fe dopants. After shifting both spectra to align the O 1*s* peak at 530.1 eV, the primary Fe $2p_{3/2}$ peak is shifted to lower binding energy compared to the thick Fe:TiO_2 film, as shown in Fig. 6(b), indicating a reduction from Fe(III) to Fe(II).[41,42] The suppression of the Fe(III) satellite and appearance of a satellite at a position consistent with Fe(II) further supports this assignment.[43] From the weak intensity of the spectra, it is difficult to discern whether a fraction of Fe(III) remains in the film. Little or no intensity is observed at the binding energy position for Fe(0), indicating that a significant fraction

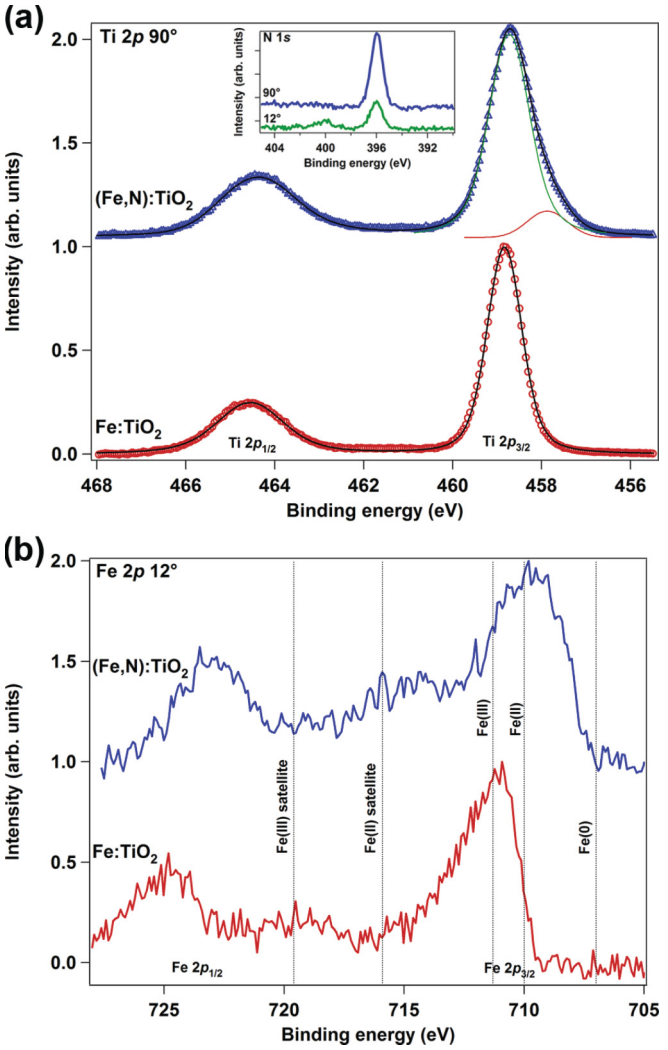

FIG. 6. (Color online) XPS core level spectra for thick Fe:TiO_2 and (Fe,N):TiO_2. All spectra have been shifted to place O 1*s* at 530.1 eV. (a) Ti 2*p* spectra collected at 90° takeoff angle (symbols) and best fit lines (solid). Inset: N 1*s* spectra at 90° and 12° for (Fe,N):TiO_2. (b) Fe 2*p* spectra collected at 12° takeoff angle. Dotted lines indicate approximate positions of known Fe spectral features for comparison.

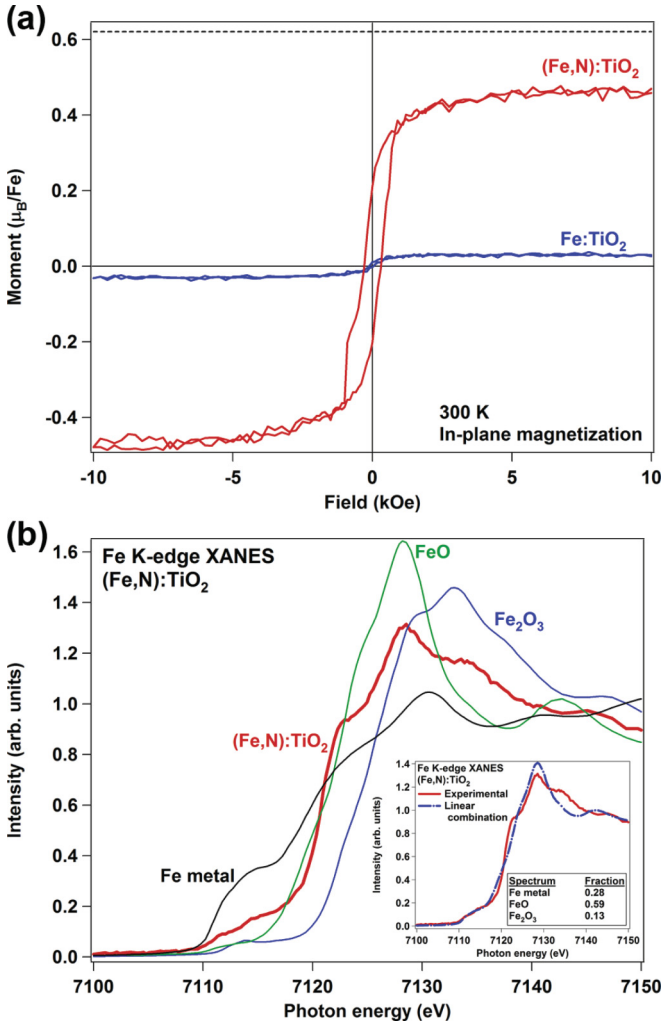

FIG. 7. (Color online) (a) VSM hysteresis loops for thick (Fe,N):TiO_2 and Fe:TiO_2 after subtraction of a linear background signal. Dotted line indicates expected saturation moment if 28% of Fe was present as Fe(0). (b) Fe K-edge XANES of thick (Fe,N):TiO_2, along with reference spectra for several Fe compounds. Inset: fit to (Fe,N):TiO_2 spectrum with a linear combination of Fe reference compounds.

of metallic Fe is not present in the near-surface region probed by XPS at a takeoff angle of 12°.

Figure 7(a) plots the room temperature hysteresis loops for 2000 Å Fe:TiO_2 and (Fe,N):TiO_2 films at room temperature. Each loop has been plotted as Bohr magnetons per Fe (μ_B/Fe), assuming the film stoichiometry is that calculated by XPS at normal takeoff angle. It should be noted that the strong surface segregation observed for the Fe:TiO_2 film may lead to an overestimation of the Fe concentration by XPS. As shown in Fig. 7(a), the saturation moment for the Fe:TiO_2 film is very small (0.03 μ_B/Fe), with no clear hysteresis. This signal likely originates from either external contamination or a very small fraction of Fe present as a secondary phase. In contrast, the saturation moment for the (Fe,N):TiO_2 film is much larger, 0.46 μ_B/Fe, with clear hystersis and a coercive field of approximately 300 Oe. However, before this magnetic signal can be attributed to uniformly distributed, substitutional Fe in TiO_2, the charge state and local environment of Fe must be further investigated.

The Fe K-edge XANES spectrum for (Fe,N):TiO_2 is shown in Fig. 7(b), along with reference standards of Fe metal, FeO, and Fe_2O_3 for comparison. In agreement with the XPS data shown in Fig. 6(b), the XANES spectrum does not indicate Fe is present as exclusively Fe(III). Instead, the leading absorption edge is consistent with a substantial fraction of Fe(II), and the intensity in the region before the absorption edge implies a significant fraction of Fe(0) is present. The reduced state of Fe is consistent with the blue color of the film after deposition. The observation of Fe(0) by XANES but not by XPS at low takeoff angle indicates that the Fe(0) is present deeper in the film, not at the surface. The fraction of Fe(0) can be estimated by fitting the pre-edge and leading-edge XANES regions with a linear combination of XANES spectra from Fe metal, FeO, and Fe_2O_3. As shown in the inset to Fig. 7(b), the best fit to the experimental data is achieved with 28% Fe(0) from Fe metal,

59% Fe(II) from FeO, and 13% Fe(III) from Fe_2O_3. It is clear that the linear combination of Fe metal, FeO, and Fe_2O_3 does not exactly reproduce the experimental spectrum, indicating that Fe may be present in other phases. However, since the position of the leading absorption edge is reasonably well reproduced by the linear combination, the fit can be taken as a rough estimate of the various charge states of Fe present in the film. If 28% of the Fe dopants are present as metallic clusters which are ferromagnetically ordered with bulk magnetic properties (2.22 μ_B/Fe), and the remaining Fe dopants are not magnetically ordered, an apparent magnetic moment of 0.62 μ_B/Fe for the (Fe,N):TiO_2 film would result. This value is indicated in Fig. 7(a) as a dotted line. Since the measured saturation moment for the (Fe,N):TiO_2 film does not exceed this value, it can be reasonably concluded that the Fe(II) and/or Fe(III) dopants are not ferromagnetically ordered, and the magnetic signal originates solely from Fe(0) secondary phases.

Coey *et al.*[13] found that room temperature ferromagnetism does not occur for fully oxidized Fe-doped rutile thin films prepared by pulsed laser deposition on $Al_2O_3(1\bar{1}02)$. Instead, the authors postulate that ferromagnetic ordering is mediated by defects present in reduced films; this mechanism requires a charge reservoir to facilitate magnetic ordering. The charge reservoir was hypothesized to be the mixed valent Fe(II)/Fe(III) present in reduced Fe:TiO_2/Al_2O_3 films. The magnetic results presented above can be compared to this model. The lack of ferromagnetic ordering in the fully oxidized Fe:TiO_2 film is consistent with the results of Coey *et al*. However, the lack of ferromagnetic ordering for the (Fe,N):TiO_2 film, beyond that predicted for the Fe(0) secondary phase, is not consistent with the charge reservoir model. From the fitting of the XANES spectrum, it is likely that at least some regions of mixed valent Fe(II)/Fe(III) are present, but these regions do not appear to have facilitated ferromagnetic ordering.

IV. CONCLUSIONS

Homoepitaxial Fe:TiO_2 and (Fe,N):TiO_2 thin films deposited on rutile TiO_2(110) were investigated by XAS and associated theoretical simulations to elucidate the detailed structure of the doped materials. Ti K-edge XANES and L-edge XAS, as well as O K-edge XANES, confirmed that the films possessed a high-quality rutile structure which was free from significant defects, disorder, and oxygen vacancies. Fe L-edge XAS ruled out secondary phases such as Fe_2O_3, Fe_3O_4, and $FeTiO_3$, although substitutional Fe in the rutile lattice could not be confirmed. The presence of a strong N K-edge XLD signal in the epitaxial film, similar to the O K-edge XLD signal, indicated conclusively that N is substitutional for O in the rutile lattice. Due to the single-crystal orientation of the epitaxial films, secondary phases such as TiN could be ruled out, in contrast to studies of randomly oriented N:TiO_2 nanoparticles. Careful analysis of the polarized N K-edge XANES spectra, and comparison with theoretical simulations, indicated that N is present in more than one local environment in the films. Although codoping with N was shown to significantly enhance Fe incorporation in rutile, the observed room temperature ferromagnetism for (Fe,N):TiO_2 was shown to arise entirely from the presence of Fe metal secondary phases. No intrinsic ferromagnetism was observed despite the presence of mixed-valent Fe(II)/Fe(III) in the (Fe,N):TiO_2 film.

ACKNOWLEDGMENTS

The authors wish to thank N. Govind for providing relaxed N:TiO_2 and (Fe,N):TiO_2 structures for the XLD simulations. A.N. gratefully acknowledges financial support from the German Research Foundation (DFG) within the Heisenberg-Programm. Use of the Advanced Photon Source, an Office of Science User Facility operated for the U.S. DOE Office of Science by Argonne National Laboratory, was supported by the U.S. DOE under Contract No. DE-AC02-06CH11357. A portion of this research was performed using EMSL, a national scientific user facility sponsored by the USDOE's Office of Biological and Environmental Research and located at the Pacific Northwest National Laboratory. Film deposition was supported by the U.S DOE, Office of Science, Office of Basic Energy Sciences, Division of Chemical Sciences, and magnetic characterization was supported by the U.S DOE, Office of Science, Office of Basic Energy Sciences, Division of Materials Sciences and Engineering.

*Corresponding author: tiffany.kaspar@pnl.gov

†Present address: Department of Solid State Physics, Johannes Kepler University, A-4040 Linz, Austria.

[1]X. Chen and S. S. Mao, Chem. Rev. **107**, 2891 (2007).

[2]O. Carp, C. L. Huisman, and A. Reller, Prog. Solid State Chem. **32**, 33 (2004).

[3]R. Asahi, T. Morikawa, T. Ohwaki, K. Aoki, and Y. Taga, Science **293**, 269 (2001).

[4]C. Di Valentin, E. Finazzi, G. Pacchioni, A. Selloni, S. Livraghi, M. C. Paganini, and E. Giamello, Chem. Phys. **339**, 44 (2007).

[5]N. Serpone, J. Phys. Chem. B **110**, 24287 (2006).

[6]Z. Z. Zhang, X. X. Wang, J. L. Long, Q. A. Gu, Z. X. Ding, and X. Z. Fu, J. Catal. **276**, 201 (2010).

[7]A. Braun, K. K. Akurati, G. Fortunato, F. A. Reifler, A. Ritter, A. S. Harvey, A. Vital, and T. Graule, J. Phys. Chem. C **114**, 516 (2010).

[8]B. Naik and K. M. Parida, Ind. Eng. Chem. Res. **49**, 8339 (2010).

[9]M. J. Yang, C. Hume, S. Lee, Y. H. Son, and J. K. Lee, J. Phys. Chem. C **114**, 15292 (2010).

[10]X. Li, Z. M. Chen, Y. C. Shi, and Y. Y. Liu, Powder Technol. **207**, 165 (2011).

[11]T. Ohno, Z. Miyamoto, K. Nishijima, H. Kanemitsu, and X. Y. Feng, Appl. Catal. A-Gen. **302**, 62 (2006).

[12]S. J. Pearton, W. H. Heo, M. Ivill, D. P. Norton, and T. Steiner, Semicond. Sci. Technol. **19**, R59 (2004).

[13]J. M. D. Coey, P. Stamenov, R. D. Gunning, M. Venkatesan, and K. Paul, New J. Phys. **12**, 053025 (2010).

[14]K. Bapna, R. J. Choudhary, S. K. Pandey, D. M. Phase, S. K. Sharma, and M. Knobel, Appl. Phys. Lett. **99**, 112502 (2011).

[15]Y. J. Kim, S. Thevuthasan, T. Droubay, A. S. Lea, C. M. Wang, V. Shutthanandan, S. A. Chambers, R. P. Sears, B. Taylor, and B. Sinkovic, Appl. Phys. Lett. **84**, 3531 (2004).

[16] A. N. Mangham, N. Govind, M. E. Bowden, V. Shutthanandan, A. G. Joly, M. A. Henderson, and S. A. Chambers, J. Phys. Chem. C **115**, 15416 (2011).
[17] S. J. Stewart, M. Fernandez-Garcia, C. Belver, B. S. Mun, and F. G. Requejo, J. Phys. Chem. B **110**, 16482 (2006).
[18] H. Y. Chen, A. Nambu, W. Wen, J. Graciani, Z. Zhong, J. C. Hanson, E. Fujita, and J. A. Rodriguez, J. Phys. Chem. C **111**, 1366 (2007).
[19] E. Sarigiannidou, F. Wilhelm, E. Monroy, R. M. Galera, E. Bellet-Amalric, A. Rogalev, J. Goulon, J. Cibert, and H. Mariette, Phys. Rev. B **74**, 041306 (2006).
[20] A. Ney, K. Ollefs, S. Ye, T. Kammermeier, V. Ney, T. C. Kaspar, S. A. Chambers, F. Wilhelm, and A. Rogalev, Phys. Rev. Lett. **100**, 157201 (2008).
[21] S. M. Heald and E. A. Stern, Phys. Rev. B **16**, 5549 (1977).
[22] F. Wilhelm, N. Jaouen, A. Rogalev, W. G. Stirling, R. Springell, S. W. Zochowski, A. M. Beesley, S. D. Brown, M. F. Thomas, G. H. Lander, S. Langridge, R. C. C. Ward, and M. R. Wells, Phys. Rev. B **76**, 024425 (2007).
[23] Y. Joly, Phys. Rev. B **63**, 125120 (2001).
[24] U. Diebold, Surf. Sci. Rep. **48**, 53 (2003).
[25] Y. Joly, D. Cabaret, H. Renevier, and C. R. Natoli, Phys. Rev. Lett. **82**, 2398 (1999).
[26] F. Farges, G. E. Brown, and J. J. Rehr, Phys. Rev. B **56**, 1809 (1997).
[27] T. Yamamoto, X-Ray Spectrom. **37**, 572 (2008).
[28] D. Cabaret, A. Bordage, A. Juhin, M. Arfaoui, and E. Gaudry, Phys. Chem. Chem. Phys. **12**, 5619 (2010).
[29] F. M. F. de Groot, M. O. Figueiredo, M. J. Basto, M. Abbate, H. Petersen, and J. C. Fuggle, Phys. Chem. Miner. **19**, 140 (1992).
[30] P. Kuiper, B. G. Searle, P. Rudolf, L. H. Tjeng, and C. T. Chen, Phys. Rev. Lett. **70**, 1549 (1993).
[31] T. Droubay, G. Mursky, and B. P. Tonner, J. Electron Spectrosc. Relat. Phenom. **84**, 159 (1997).
[32] A. Agui, M. Mizumaki, Y. Saitoh, T. Matsushita, T. Nakatani, A. Fukaya, and E. Torikai, J. Synchrotron Radiat. **8**, 907 (2001).
[33] J. G. Chen, Surf. Sci. Rep. **30**, 1 (1997).
[34] F. M. F. de Groot, J. Faber, J. J. M. Michiels, M. T. Czyzyk, M. Abbate, and J. C. Fuggle, Phys. Rev. B **48**, 2074 (1993).
[35] R. Ruus, A. Kikas, A. Saar, A. Ausmees, E. Nommiste, J. Aarik, A. Aidla, T. Uustare, and I. Martinson, Solid State Commun. **104**, 199 (1997).
[36] F. Esaka, K. Furuya, H. Shimada, M. Imamura, N. Matsubayashi, H. Sato, A. Nishijima, A. Kawana, H. Ichimura, and T. Kikuchi, J. Vac. Sci. Technol. A **15**, 2521 (1997).
[37] N. C. Saha and H. G. Tompkins, J. Appl. Phys. **72**, 3072 (1992).
[38] R. T. Haasch, T.-Y. Lee, D. Gall, J. E. Greene, and I. Petrov, Surf. Sci. Spectra **7**, 193 (2000).
[39] S. A. Chambers, S. H. Cheung, V. Shutthanandan, S. Thevuthasan, M. K. Bowman, and A. G. Joly, Chem. Phys. **339**, 27 (2007).
[40] J. J. Yeh and I. Lindau, At. Data Nucl. Data Tables **32**, 1 (1985).
[41] Y. Gao, Y. J. Kim, S. A. Chambers, and G. Bai, J. Vac. Sci. Technol. A **15**, 332 (1997).
[42] T. Schedel-Niedrig, W. Weiss, and R. Schlogl, Phys. Rev. B **52**, 17449 (1995).
[43] M. Muhler, R. Schlogl, and G. Ertl, J. Catal. **138**, 413 (1992).